FERMILAB-PUB-20-493-AD-SCD

EUROPEAN ORGANISATION FOR NUCLEAR RESEARCH (CERN)

CERN-EP-2020-142
September 7, 2020

Measurements of multiplicity fluctuations of identified hadrons in inelastic proton-proton interactions at the CERN Super Proton Synchrotron

The NA61/SHINE Collaboration

Measurements of multiplicity fluctuations of identified hadrons produced in inelastic p+p interactions at 31, 40, 80, and 158 GeV/c beam momentum are presented. Four different measures of multiplicity fluctuations are used: the scaled variance ω and strongly intensive measures Σ, Φ and Δ. These fluctuation measures involve second and first moments of joint multiplicity distributions. Data analysis is preformed using the Identity method which corrects for incomplete particle identification. Strongly intensive quantities are calculated in order to allow for a direct comparison to corresponding results on nucleus-nucleus collisions. The results for different hadron types are shown as a function of collision energy. A comparison with predictions of string-resonance Monte-Carlo models: Epos, Smash and Venus, is also presented.

This document was prepared by NA61/SHINE collaboration using the resources of the Fermi National Accelerator Laboratory (Fermilab), a U.S. Department of Energy, Office of Science, HEP User Facility. Fermilab is managed by Fermi Research Alliance, LLC (FRA), acting under Contract No. DE-AC02-07CH11359.

1 Introduction

This paper presents experimental results on event-by-event fluctuations of multiplicities of identified particles produced in inelastic proton-proton (p+p) interactions at 31, 40, 80, and 158 GeV/c ($\sqrt{s_{\mathrm{NN}}}$ = 7.6, 8.7, 12.3, 17.3 GeV). The measurements were performed by the multi-purpose NA61/SHINE [1] experiment at the CERN Super Proton Synchrotron (SPS) in 2009. They are part of the strong interactions programme devoted to the study of the properties of the onset of deconfinement and search for the critical point of strongly interacting matter. Within this program, a two dimensional scan in collision energy and size of colliding nuclei was performed [2].

An interpretation of the experimental results on nucleus-nucleus (A+A) collisions relies to a large extent on a comparison with the corresponding data on p+p and p+A interactions. However, available results on fluctuations of identified hadrons in these reactions are sparse. Moreover, fluctuation measurements cannot be corrected in a model independent manner for partial phase-space acceptance. Thus all measurements of the scan should be performed in the same phase space region. This motivated the NA61/SHINE Collaboration to analyse data on p+p interactions with respect to fluctuations using the same experimental methods, acceptance and measures as used to study nucleus-nucleus collisions.

Fluctuations in A+A collisions are susceptible to two trivial sources: the finite and fluctuating number of produced particles and event-by-event fluctuations of the collision geometry. Suitable statistical tools have to be chosen to extract the fluctuations of interest. In this publication four different event-by-event fluctuation measures are used: the scaled variance ω, the Φ quantity [3], and the Δ and Σ measures introduced in Refs. [4, 5]. They were already successfully utilized by the NA49 experiment at the CERN SPS, see e.g. Refs. [6, 7, 8, 9, 10, 11, 12] and NA61/SHINE, see e.g. Ref. [13].

Experimental measurements of multiplicity distributions of identified hadrons are challenging because it is often impossible to identify a particle with sufficient precision. In this paper the *Identity method* [14, 15, 16, 17, 18, 19] is employed to circumvent this problem. The Identity method has already been successfully used in the past by collaborations NA49 [9], NA61/SHINE [20], and ALICE [21, 22, 23].

The paper is organized as follows. In Sec. 2 intensive and strongly intensive measures of fluctuations used in this analysis are introduced and briefly discussed. The Identity method which allows to take into account the incomplete particle identification is presented in Sec. 3. The NA61/SHINE set-up and the data reconstruction method are presented in Secs. 4 and 5, respectively. The data analysis procedure is introduced in Secs. 6, 7 and 8. Applied corrections and remaining uncertainties are presented in Sec. 9. Results on the collision energy dependence of multiplicity fluctuations of identified hadrons in inelastic p+p collisions at 31, 40, 80, and 158 GeV/c beam momentum are presented, discussed and compared with model predictions in Sec. 10. A summary closes the paper.

Throughout this paper the rapidity is calculated in the collision center of mass system: $y = \mathrm{atanh}(\beta_L)$, where $\beta_L = p_L/E$ is the longitudinal (z) component of the velocity, p_L and E are particle longitudinal

momentum and energy given in the collision center of mass system. The transverse component of the momentum is denoted as p_T and the azimuthal angle ϕ is the angle between the transverse momentum vector and the horizontal (x) axis. Total momentum in the laboratory system is denoted as p_{lab}. The collision energy per nucleon pair in the center of mass system is denoted as $\sqrt{s_{\mathrm{NN}}}$, respectively.

2 Intensive and strongly intensive measures of multiplicity and particle type fluctuations

2.1 Intensive quantities

Measures of multiplicities and fluctuations are called intensive when they are *independent* of the volume (V) of systems modelled by the ideal Boltzmann grand canonical ensemble (IB-GCE). In contrast, extensive quantities (for example mean multiplicity or variance of the multiplicity distribution) are proportional to the system volume within IB-GCE. One can also extend the notion of intensive and extensive quantities to the Wounded Nucleon Model (WNM) [24], where the intensive quantities are those which are independent of the number of wounded nucleons (W), and extensive those which are proportional to the number of wounded nucleons. Here it is assumed that the number of wounded nucleons is the same for all collisions. The ratio of two extensive quantities is an intensive quantity [4]. Therefore, the ratio of mean multiplicities N_a and N_b, as well as the scaled variance of the multiplicity distribution $\omega[a] \equiv (\langle N_a^2\rangle - \langle N_a\rangle^2)/\langle N_a\rangle$, are intensive measures. As a matter of fact, due to its intensity property, the scaled variance of the multiplicity distribution $\omega[a]$ is widely used to quantify multiplicity fluctuations in high-energy heavy-ion experiments.

The scaled variance takes the value $\omega[a] = 0$ for $N_a = const.$ and $\omega[a] = 1$ for a Poisson distribution of N_a.

2.2 Strongly intensive quantities

In nucleus-nucleus collisions the volume of the produced matter (or number of wounded nucleons) cannot be fixed – it changes from one event to another. The quantities, which within the IB-GCE (or WNM) model are independent of V (or W) fluctuations are called *strongly intensive* quantities [3, 4]. The ratio of mean multiplicities is both an intensive and a strongly intensive quantity, whereas the scaled variance is an intensive but not strongly intensive quantity.

Strongly intensive quantities Δ and Σ used in this paper are defined as [5]:

$$\Delta[a,b] \equiv \frac{1}{\langle N_b\rangle - \langle N_a\rangle} \cdot \Big(\langle N_b\rangle\omega[a] - \langle N_a\rangle\omega[b]\Big) \tag{1}$$

and

$$\Sigma[a,b] \equiv \frac{1}{\langle N_b\rangle + \langle N_a\rangle} \cdot \Big[\langle N_b\rangle\omega[a] + \langle N_a\rangle\omega[b] - 2\Big(\langle N_a N_b\rangle - \langle N_a\rangle\langle N_b\rangle\Big)\Big], \tag{2}$$

where N_a and N_b stand for multiplicities of particles of type a and b, respectively. First and second pure moments, $\langle N_a\rangle$, $\langle N_b\rangle$, and $\langle N_a^2\rangle$, $\langle N_b^2\rangle$ define $\Delta[a,b]$. In addition, the second mixed moment, $\langle N_a N_b\rangle$, is needed to calculate $\Sigma[a,b]$.

The first strongly intensive quantity Φ was introduced in 1992 [3] and can be expressed via Σ:

$$\Phi[a,b] = \frac{\sqrt{\langle N_a\rangle\langle N_b\rangle}}{\langle N_a + N_b\rangle} \cdot \Big(\sqrt{\Sigma[a,b]} - 1\Big). \tag{3}$$

With the normalization of Δ and Σ used here [5], the quantities $\Delta[a,b]$ and $\Sigma[a,b]$ are dimensionless and have a common scale required for a quantitative comparison of fluctuations of different, in general dimensional, extensive quantities. More precisely, the values of Δ and Σ are equal to zero in the absence of event-by-event fluctuations ($N_a = const.$, $N_b = const.$) and equal to one for fluctuations given by the model of independent particle production (Independent Particle Model) [5].

3 Identity method

Experimental measurement of a joint multiplicity distribution of identified hadrons is challenging. Typical tracking detectors, like time projection chambers used by NA61/SHINE, allow for a precise measurement of momenta of charged particles and sign of their electric charges. In order to be able to distinguish between different particle types (e.g. a particle type a being e^+, π^+, K^+ or p) a determination of particle mass is necessary. This is done indirectly by measuring for each particle a value of the specific energy loss dE/dx in the tracking detectors, the distribution of which depends on mass, momentum and charge. The resolution of dE/dx measurements is usually poor. Probabilities to register particles of different types with the same value of dE/dx are often comparable. Consequently, it is impossible to identify particles individually with reasonable confidence. The Identity method [14, 15, 16, 17, 18, 19] is a tool to measure moments of multiplicity distribution of identified particles, which circumvents the experimental issue of incomplete particle identification.

The method employs the fitted inclusive dE/dx distribution functions of particles of type a, $\rho_a(dE/dx)$ in momentum bins. Each event has a set of measured dE/dx values corresponding to each track in the event. For each track in an event the probability w_a of being a particle of type a is calculated:

$$w_a = \rho_a(dE/dx) \;/\; \rho(dE/dx)\;, \tag{4}$$

where

$$\rho(dE/dx) = \sum_a \rho_a(dE/dx)\;. \tag{5}$$

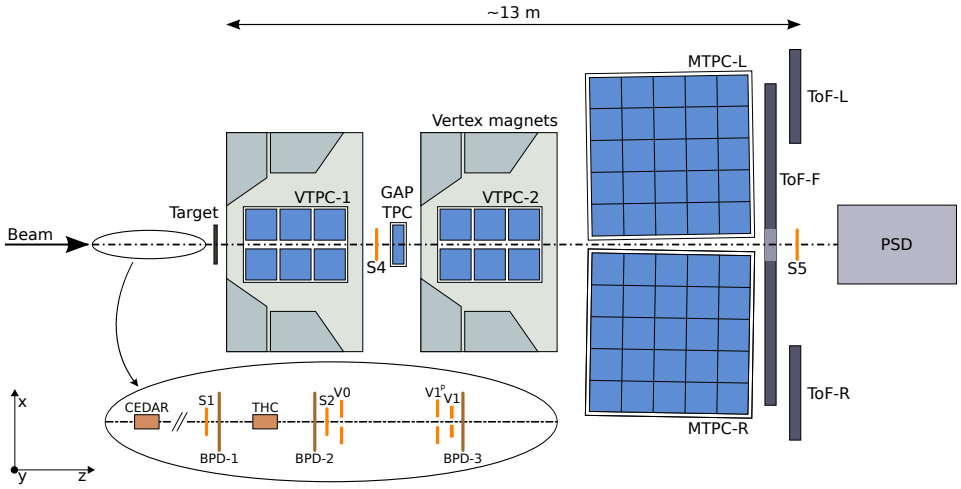

Figure 1: (Color online) The schematic layout of the NA61/SHINE experiment at the CERN SPS (horizontal cut, not to scale), see text and Ref. [1] for details.

Next, an event variable W_a (a smeared multiplicity of particle a in the event) is defined as:

$$W_a = \sum_{n=1}^{N} w_{a,n} \,, \tag{6}$$

where N is the number of measured particles in the event.

The Identity method unfolds moments of the true multiplicity distributions from moments of the smeared multiplicity distribution $P(W_a)$ using a response matrix calculated from the measured $\rho_a(\mathrm{d}E/\mathrm{d}x)$ distributions [15].

4 Experimental setup

The NA61/SHINE experimental facility [1] consists of a large acceptance hadron spectrometer located in the H2 beam line of the CERN North Area. The schematic layout of the NA61/SHINE detector is shown in Fig. 1.

The results presented in this paper were obtained using measurement from the Time Projection Chambers (TPC), the Beam Position Detectors and the beam and trigger counters. These detector components as well as the proton beam and the liquid hydrogen target are briefly described below. Further information can be found in Refs. [1, 25, 26].

For data taking on p+p interactions a liquid hydrogen target of 20.29 cm length (2.8% interaction length) and 3 cm diameter was placed 88.4 cm upstream of VTPC-1.

Secondary beams of positively charged hadrons at 31, 40, 80, and 158 GeV/c were produced from 400 GeV/c protons extracted from the SPS onto a beryllium target. A selection based on signals from a set of detectors along the H2 beam-line (scintillation counters S, Cerenkov detectors CEDAR, THC and beam position detectors BPD (see inset in Fig. 1)) allowed to identify beam protons with a purity of about 99%. A coincidence of these signals provided the beam trigger T_{beam}.

The interaction trigger T_{int} was provided by the anti-coincidence of the incoming proton beam and a scintillation counter S4 ($T_{int} = T_{beam} \wedge \overline{\mathrm{S4}}$). The S4 counter with 2 cm diameter, was placed between the VTPC-1 and VTPC-2 detectors along the beam trajectory at about 3.7 m from the target, see Fig. 1.

The main tracking devices of the spectrometer are four large volume TPCs. Two of them, the vertex TPCs (VTPC-1 and VTPC-2), are located in the magnetic fields of two super-conducting dipole magnets with a maximum combined bending power of 9 Tm which corresponds to about 1.5 T and 1.1 T fields in the upstream and downstream magnets, respectively. In order to optimize the acceptance of the detector, the fields in both magnets were adjusted proportionally to the beam momentum.

Two large main TPCs (MTPC-L and MTPC-R) are positioned downstream of the magnets symmetrically to the beam line. The fifth small TPC (GAP TPC) is placed between VTPC-1 and VTPC-2 directly on the beam line. It closes the gap between the beam axis and the sensitive volumes of the other TPCs. Simultaneous measurements of dE/dx and p_{lab} allow to extract information on particle mass, which is used to identify charged particles. Behind the MTPCs there were three Time-of-Flight (ToF) detectors.

5 Data reconstruction and simulation

The event vertex and the produced particle tracks were reconstructed using the standard NA61/SHINE software. Details on the reconstruction procedure of proton-proton interactions in NA61/SHINE can be found in Ref. [25].

Detector parameters were optimized by a data-based calibration procedure which also took into account their time dependence, for details see Refs. [25, 27].

A simulation of the NA61/SHINE detector response was used to correct the reconstructed data. Several Monte Carlo models were compared with the NA61/SHINE results on p+p, p+C and π+C interactions: Fluka2008, Urqmd1.3.1, Venus4.12, Epos1.99, Gheisha2002, QGSJetII-04 and Sibyll2.1 [25, 26, 28, 29]. Based on these comparisons and taking into account continuous support and documentation from the developers the Epos1.99 model [30, 31] was selected for the MC simulation. Generated and reconstructed tracks were matched based on the number of common points along their path. Possible differences due to the different identification procedures followed in the MC simulations and the real data are addressed in Ref. [26] and Sec. 9.3.

It should be underlined that only inelastic p+p interactions in the hydrogen of the target cell were simulated and reconstructed. Thus the MC based corrections (see Sec. 9.1) can be applied only for inelastic events. The contribution of elastic events is removed by the event selection cuts (see Sec. 7).

6 Data analysis

This section starts with a brief overview of the data analysis procedure and the applied corrections. It also defines which class of particles the final results correspond to.

The analysis procedure consists of the following steps:

(i) application of event and track selection criteria,

(ii) determination of inclusive $\mathrm{d}E/\mathrm{d}x$ spectra,

(iii) determination of moments of identified hadron multiplicity distributions with the Identity method,

(iv) evaluation of corrections to the moments based on experimental data and simulations,

(v) calculation of the corrected moments and fluctuation quantities,

(vi) calculation of statistical and systematic uncertainties.

Corrections for the following biases were evaluated and applied:

(i) contribution of particles other than *primary* (see below) hadrons produced in inelastic p+p interactions,

(ii) losses of primary hadrons due to measurement inefficiencies,

(iii) losses of inelastic p+p interactions due to the trigger and the event and track selection criteria employed in the analysis

The final results refer to identified hadrons produced in inelastic p+p interactions by strong interaction processes and in electromagnetic decays of produced hadrons. Such hadrons are referred to as *primary* hadrons.

The analysis was performed in the kinematic acceptance limited by the detector geometry and the statistics of inclusive $\mathrm{d}E/\mathrm{d}x$ spectra. The acceptance is given in the form of two sets of tables:

(i) three-dimensional tables representing the high efficiency region of the detector,

(ii) two-dimensional tables defining the $\mathrm{d}E/\mathrm{d}x$ fit range.

The acceptance tables can be found in Ref. [32].

7 Event and track selection

7.1 Event selection

Inelastic p+p events were selected using the following criteria:

(i) no off-time beam particle detected within a time window of ± 1.5 μs around the trigger particle,

(ii) beam particle trajectory measured in at least three planes out of four of BPD-1 and BPD-2 and in both planes of BPD-3,

(iii) the primary interaction vertex fit converged,

(iv) z position of the interaction vertex (fitted using the beam trajectory and TPC tracks) not further away than 20 cm from the center of the liquid hydrogen target (LHT),

(v) events with a single, positively charged track with absolute momentum close to the beam momentum (see Ref. [25]) are removed in order to eliminate elastic scattering reactions.

7.2 Track selection

In order to select tracks of primary charged hadrons and to reduce the contamination of tracks from secondary interactions, weak decays and off-time interactions, the following track selection criteria were applied:

(i) track momentum fit at the interaction vertex should have converged,

(ii) total number of reconstructed points on the track should be greater than 30,

(iii) sum of the number of reconstructed points in VTPC-1 and VTPC-2 should be greater than 15 or the number of reconstructed points in the GAP TPC should be greater than 4,

(iv) the distance between the track extrapolated to the interaction plane and the interaction point (impact parameter) should be smaller than 4 cm in the horizontal (bending) plane and 2 cm in the vertical (drift) plane,

(v) the total number of reconstructed dE/dx points on the track should be greater than 30,

(vi) the track lies in the high efficiency region of the detector and the dE/dx fit acceptance maps given in Ref. [32].

The event and track statistics after applying the selection criteria are summarized in Table 1.

Table 1: Statistics of accepted events as well as number of accepted positively and negatively charged tracks for data sets analysed in the paper.

Beam momentum [GeV/c]	# events	# positively charged tracks	# negatively charged tracks
31	819710	530971	132187
40	2641412	2071490	675258
80	1531849	2061069	1020267
158	1587680	3243819	1980037

8 Identity analysis

In order to calculate moments of multiplicity distributions of identified hadrons corrected for incomplete particle identification the analysis was performed using the Identity method. The analysis consists of three steps:

(i) parametrization of inclusive dE/dx spectra,

(ii) calculation of smeared multiplicity distributions and their moments,

(iii) correcting smeared moments for incomplete particle identification using the dE/dx response matrix.

The Identity analysis steps are briefly described below.

8.1 Parametrization of dE/dx spectra

For each particle its specific energy loss dE/dx is calculated as the truncated mean (smallest 50%) of cluster charges measured along the track trajectory. As an example, dE/dx measured in p+p interactions at 80 GeV/c, for positively and negatively charged particles, as a function of $q \times p_{\mathrm{lab}}$ is presented in Fig. 2. The expected mean values of dE/dx for different particle types are shown by the Bethe-Bloch curves.

The parametrization of dE/dx spectra of e^+, e$^-$, π^+, π^-, K^+, K^-, p, and $\bar{\mathrm{p}}$ were obtained by fitting the dE/dx distributions separately for positively and negatively charged particles in bins of p_{lab} and transverse momentum p_{T} with a sum of four functions [26, 33, 34] each corresponding to the expected dE/dx distribution for a given particle type. The details of this fitting procedure can be found in Ref. [26]. In contrast to spectra analysis [26] separate fits were performed in order to extend acceptance by adding particles with negative $p_{\mathrm{lab,x}}/q$. Systematic uncertainties arising from the fitting procedure are estimated in Sec. 9.

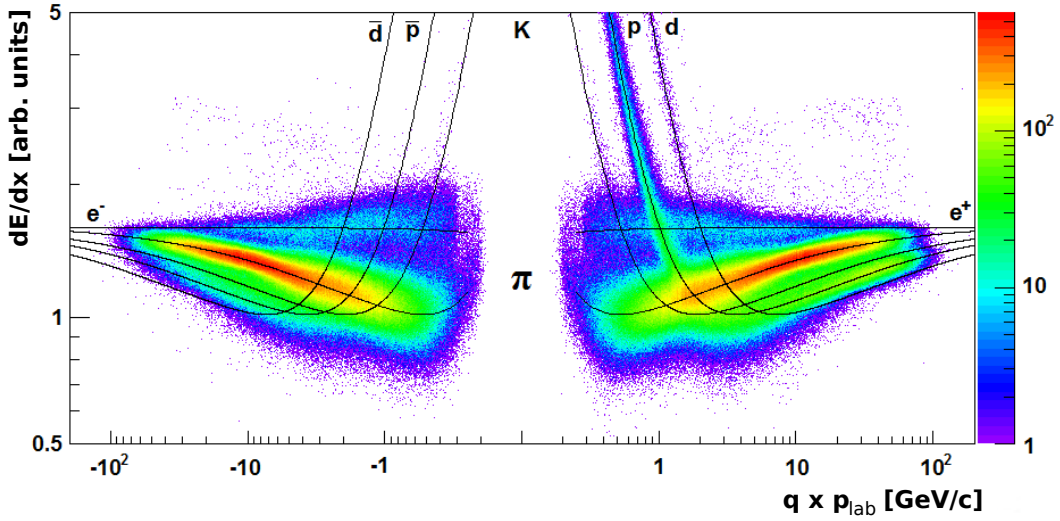

Figure 2: (Color online) Distribution of charged particles in the dE/dx- $q \times p_{\mathrm{lab}}$ (q represents electric charge) plane. The energy loss in the TPCs for different charged particles for events and tracks selected for the analysis of p+p interactions at 80 GeV/c. Expectations for the dependence of the mean dE/dx on p_{lab} for the considered particle types are shown by the curves calculated based on the Bethe-Bloch function.

In order to ensure similar particle numbers in each bin, 20 logarithmic bins were chosen in p_{lab} in the range 1−100 GeV/c. Furthermore, the data were binned in 20 equal p_{T} intervals in the range 0−2 GeV/c.

The dE/dx spectrum for a given particle type was parametrized by the sum of asymmetric Gaussians with widths $\sigma_{a,l}$ depending on the particle type a and the number of points l measured in the TPCs. Simplifying the notation in the fit formulae, the peak position of the dE/dx distribution for particle type a is denoted as x_a. The contribution of a reconstructed particle track to the fit function reads:

$$f(x) = \sum_a f_a(x) = \sum_{a=\pi,\mathrm{p,K,e}} Y_a \frac{1}{\sum_l n_l} \sum_l \frac{n_l}{\sqrt{2\pi}\sigma_l} \exp\left[-\frac{1}{2}\left(\frac{x - x_a}{(1 \pm \delta)\sigma_l}\right)^2\right], \tag{7}$$

where x is the dE/dx of the particle, n_l is the number of tracks with number of points l in the sample and Y_a is the amplitude of the contribution of particles of type a. The second sum is the weighted average of the line-shapes from the different numbers of measured points (proportional to track-length) in the sample. The quantity σ_l is written as:

$$\sigma_l = \sigma_0 \left(\frac{x_i}{x_\pi}\right)^{0.625} \Big/ \sqrt{l}\,, \tag{8}$$

where the width parameter σ_0 is assumed to be common for all particle types and bins. A $1/\sqrt{l}$ dependence on number of points is assumed. The Gaussian peaks are allowed to be asymmetric to describe the tail of the Landau distribution which may still be present after truncation.

Examples of fits for p+p interactions at 31 and 158 GeV/c are shown in Fig. 3.

In order to ensure good fit quality, only bins with number of tracks greater than 500 were used for further analysis. The Bethe-Bloch curves for different particle types cross each other at low values of the total momentum. Thus, the proposed technique is not sufficient for particle identification at low p_{lab} and bins with $p_{\mathrm{lab}} < 4.3$ GeV/c were excluded from this analysis based solely on dE/dx.

The requirement of at least 500 tracks with good quality dE/dx measurement in each p_{lab}, p_{T} bin reduces the acceptance available for the analysis. Due to different multiplicities the acceptance is different for positively and negatively charged particles. Moreover, it also changes with beam momentum. Thus, the largest acceptance was found for positively charged hadrons at 158 GeV/c and the smallest at 31 GeV/c for negatively charged hadrons. The acceptance used in this analysis is given separately for negatively and positively charged particles by a set of publicly available acceptance tables [32]. The corresponding rapidity and transverse momentum acceptances at 31 and 158 GeV/c are shown in Fig. 4.

8.2 Smeared moments of multiplicity distribution

The parametrization of inclusive dE/dx spectra of identified particles is first used to calculate the particle identities w_a (see Sec. 3). Distributions of w_a for p+p interactions at 31 and 158 GeV/c are shown in Figs. 5 and 6 for positively and negatively charged particles, separately.

In the second step smeared multiplicities of identified particles W_a (see Sec. 3) are calculated for each selected event and their distributions are obtained. Examples of smeared multiplicity distributions for p+p interactions at 31 and 158 GeV/c are shown in Figs. 7 and 8 for positively and negatively charged particles, separately.

Finally, first and second moments of smeared multiplicity distributions are calculated: $\langle W_p \rangle$, $\langle W_K \rangle$, $\langle W_\pi \rangle$, $\langle W_e \rangle$, $\langle W_p^2 \rangle$, $\langle W_K^2 \rangle$, $\langle W_\pi^2 \rangle$, $\langle W_e^2 \rangle$, $\langle W_p W_K \rangle$, $\langle W_p W_\pi \rangle$, $\langle W_p W_e \rangle$, $\langle W_K W_\pi \rangle$, $\langle W_K W_e \rangle$, $\langle W_\pi W_e \rangle$ for positively and negatively charged particles, separately.

8.3 Correcting smeared moments for incomplete particle identification

Following the Identity method [15, 16] one calculates the first and second moments of multiplicity distributions corrected for incomplete particle identification as follows.

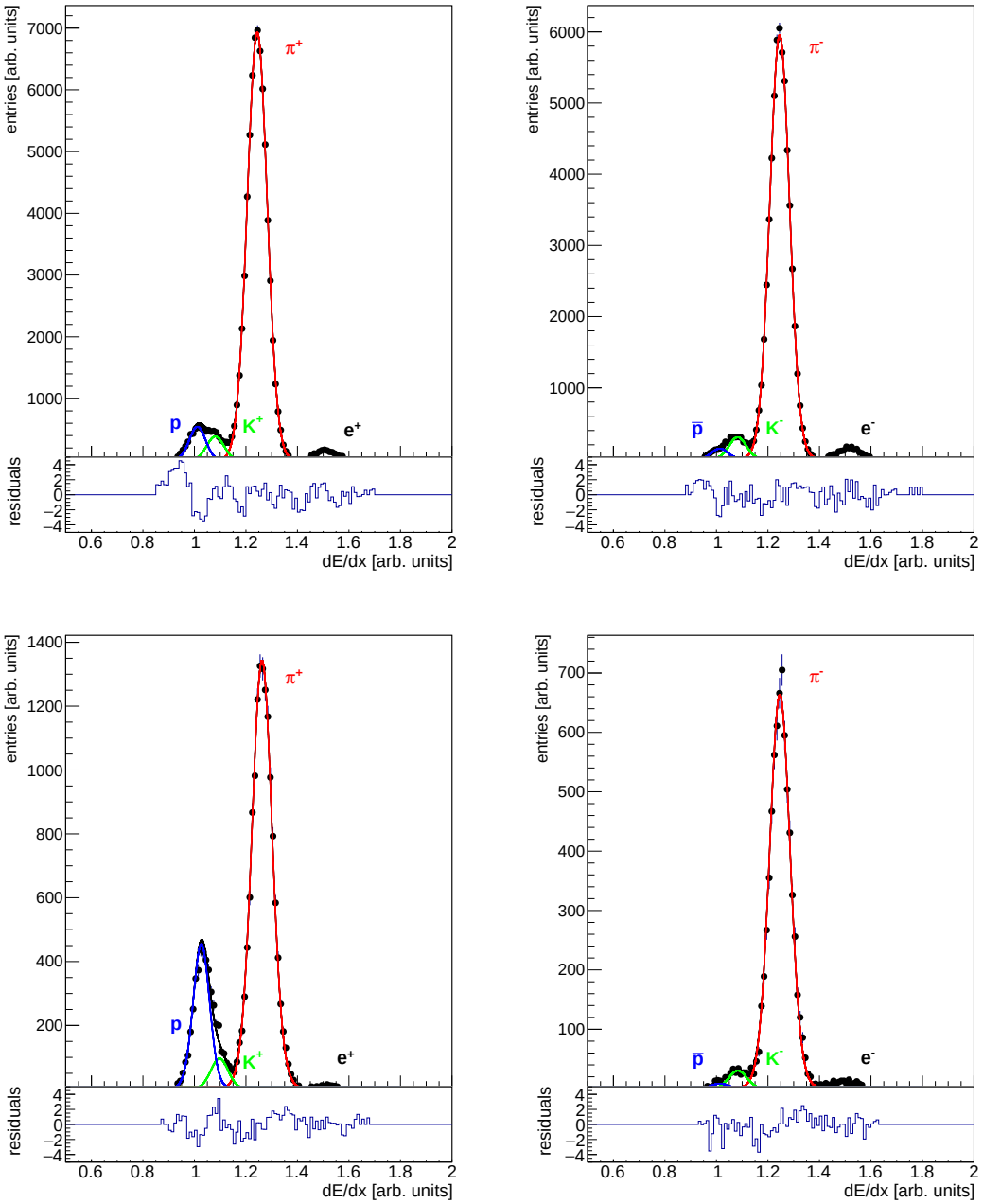

Figure 3: (Color online) The dE/dx distributions for positively (*left*) and negatively (*right*) charged particles in the bin $5.46 < p_{\rm lab} \leq 6.95$ GeV/c and $0.1 < p_{\rm T} \leq 0.2$ GeV/c produced in p+p interactions at 158 GeV/c (*top*) and 31 GeV/c (*bottom*). The fit by a sum of contributions from different particle types is shown by black lines. The corresponding residuals (the difference between the data and fit divided by the statistical uncertainty of the data) is shown in the bottom plots.

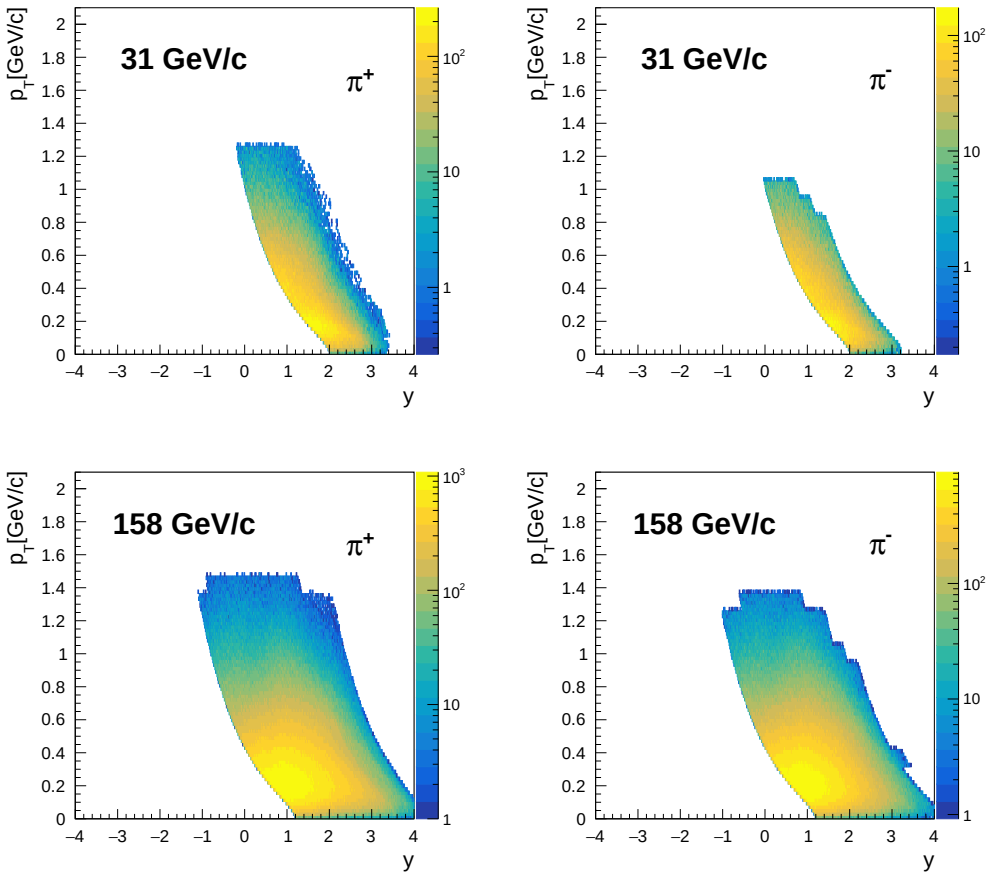

Figure 4: (Color online) Distributions of particles rapidity (calculated in the collision center-of-mass reference system assuming pion mass) and p_{T} of all particles selected for the analysis. The two upper plots are for 31 GeV/c and the two lower plots for 158 GeV/c. The irregular edges of the distributions reflect the boundaries of the p_{lab}, p_{T} bins used in the dE/dx analysis.

The first moments of the multiplicity distributions for complete particle identification, $\langle N_a \rangle$ are equal to the corresponding first moments of the smeared multiplicity distributions:

$$\langle N_a \rangle = \langle W_a \rangle \, . \tag{9}$$

Second moments of the multiplicity distributions of identified hadrons are obtained by solving sets of linear equations which relate them to the corresponding smeared moments. The coefficients of the equations are calculated using the identified particle densities in dE/dx. The Identity method was quantitatively tested by numerous simulations, see for example Refs. [16, 18]. Here results of a qualitative data-based test are presented.

The energy dependence of the scaled variance ω of all charged pions $\omega[\pi]$ calculated using the Identity method was compared with the scaled variance calculated for charged particles. The results are very

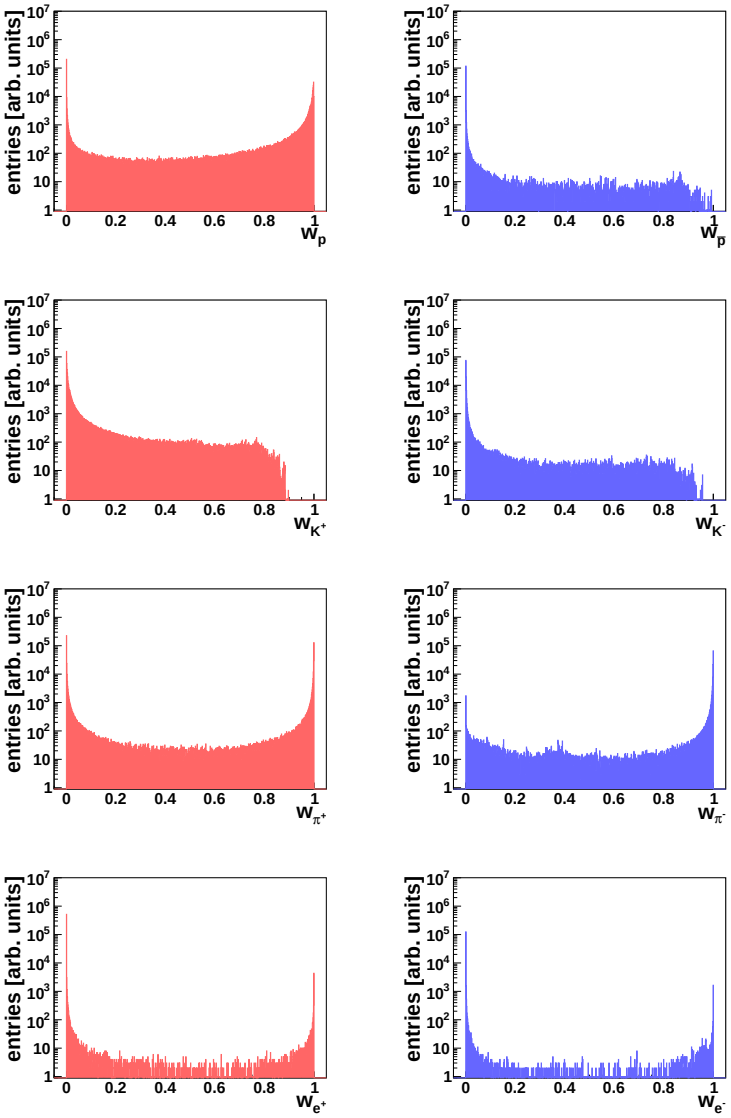

Figure 5: (Color online) Distributions of identities of positively (*left*) and negatively (*right*) charged particles (from top to bottom: p, K, π, e) selected for the analysis in p+p interactions at 31 GeV/c.

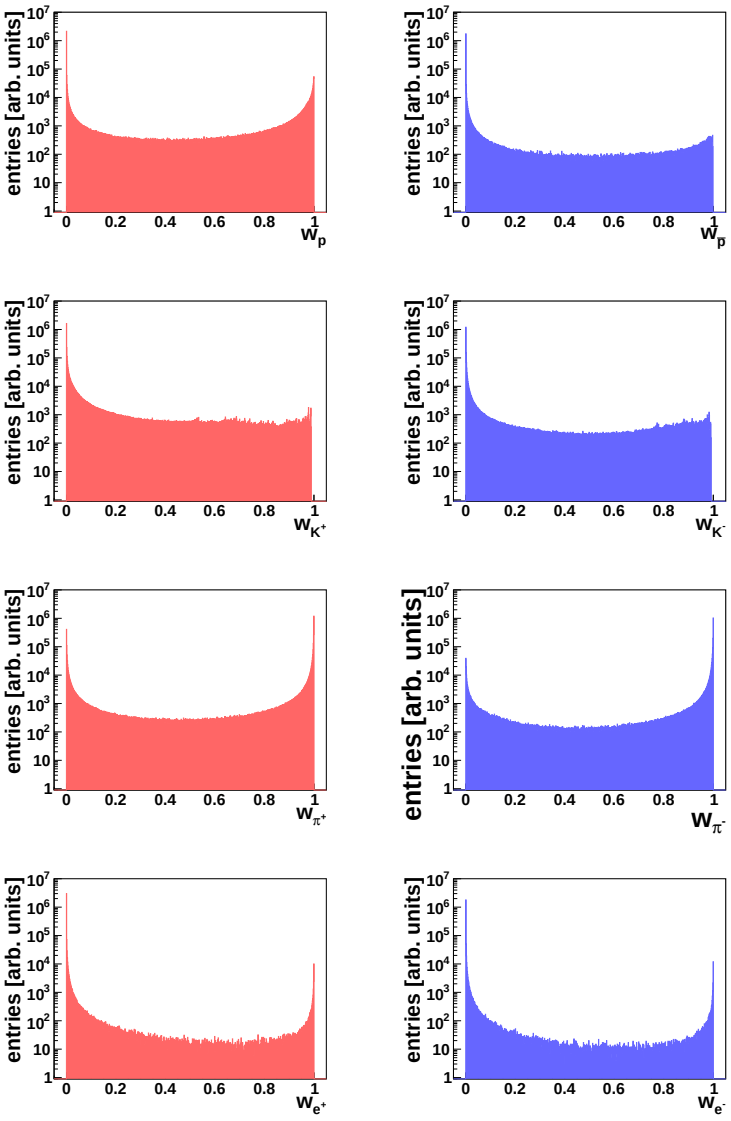

Figure 6: (Color online) Distributions of identities of positively (*left*) and negatively (*right*) charged particles (from top to bottom: p, K, π, e) selected for the analysis in p+p interactions at 158 GeV/c.

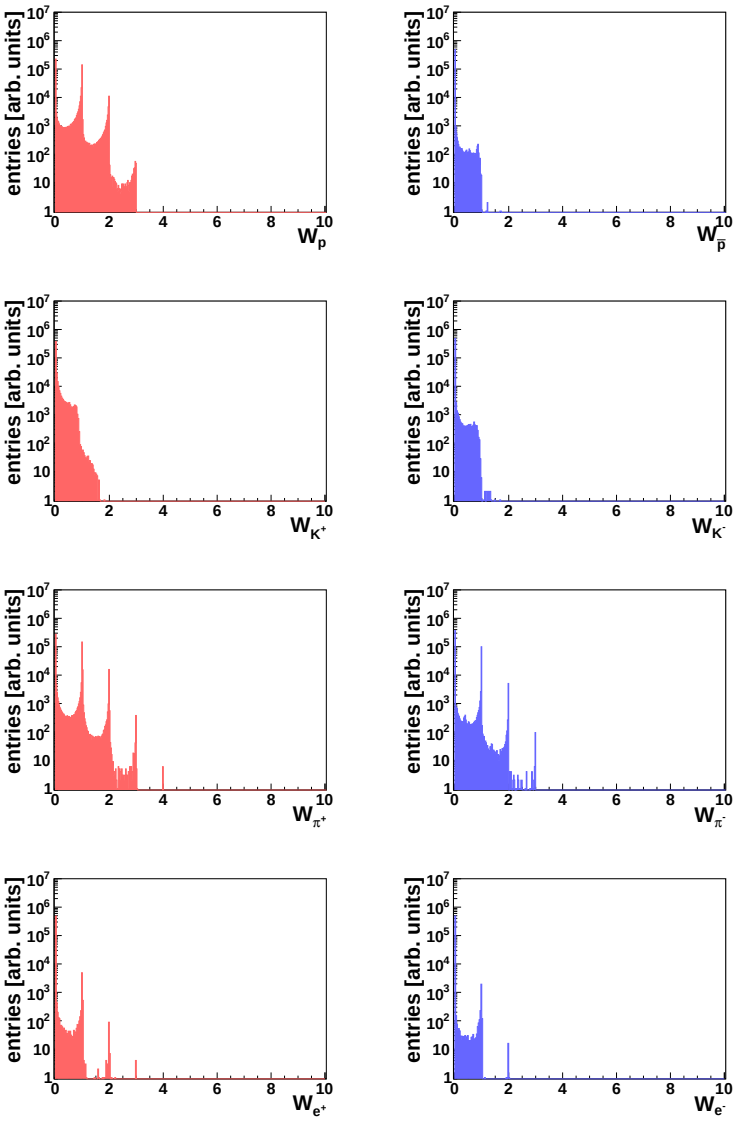

Figure 7: (Color online) Smeared multiplicity distributions of positively (*left*) and negatively (*right*) charged particles (from top to bottom: p, K, π, e) in p+p interactions at 31 GeV/c.

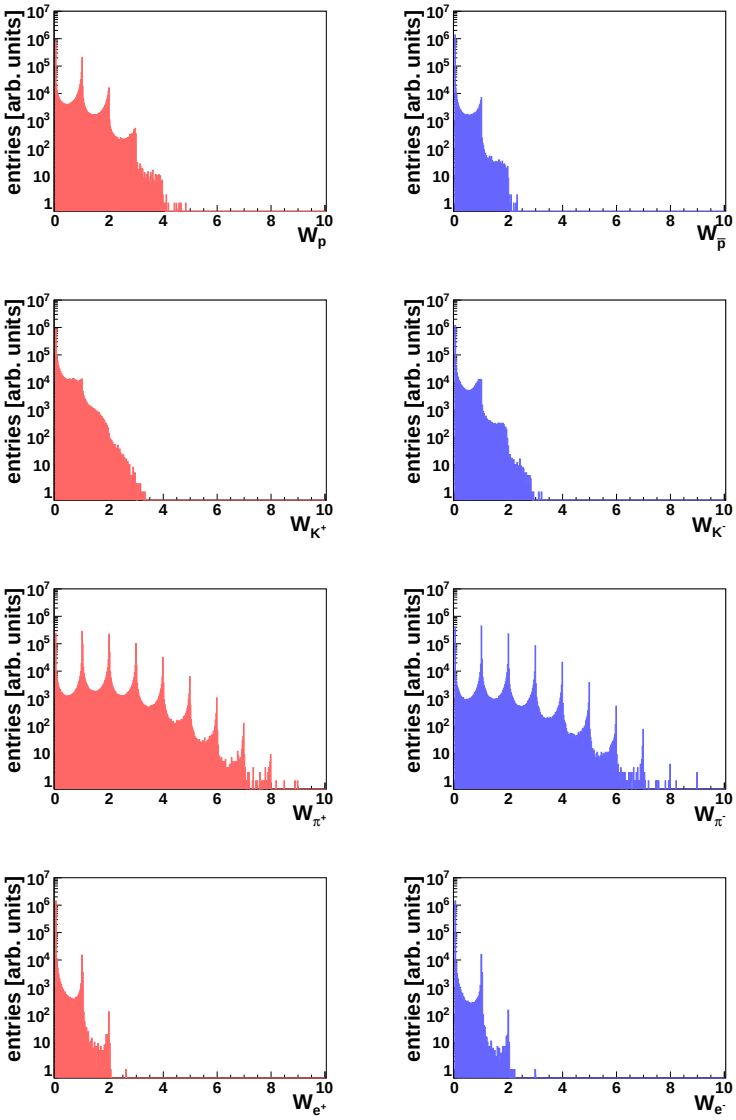

Figure 8: (Color online) Smeared multiplicity distributions of positively (*left*) and negatively (*right*) charged particles (from *top* to *bottom*: p, K, π, e) in p+p interactions at 158 GeV/c.

close at the higher collision energies where pions dominate the charged particles. This can be taken as a further validation of the Identity analysis.

9 Corrections and uncertainties

This section briefly describes the corrections for biases and presents methods to calculate statistical and systematic uncertainties.

9.1 Corrections for event and track losses and contribution of unwanted tracks

The first and second moments of multiplicity distributions corrected for incomplete particle identification were also corrected for

(i) loss of inelastic events due to the on-line and off-line event selection,

(ii) loss of particles due to the detector inefficiency and track selection,

(iii) contribution of particles from weak decays and secondary interactions (feed-down).

A simulation of the NA61/SHINE detector response was used to correct the data for the above mentioned biases. Corrections were calculated for moments of identified hadron multiplicity distributions. Events simulated with the Epos1.99 model were reconstructed with the standard NA61/SHINE software as described in Sec. 5. The multiplicative correction factors $C_a^{(k)}$ and C_{ab}, where a and b denotes particle type ($a, b = \pi^{+/-}, K^{+/-}, p, \bar{p}, e^{+/-}$; and $a \neq b$) are defined as:

$$C_a^{(k)} = \frac{(N_a^k)_{gen}^{MC}}{(N_a^k)_{sel}^{MC}}, \quad C_{ab} = \frac{(N_{ab})_{gen}^{MC}}{(N_{ab})_{sel}^{MC}}, \tag{10}$$

where:

(i) $(N_a^k)_{gen}^{MC}$ – moment $k = 1, 2$ of particle type a ($a = \pi^{+/-}, K^{+/-}, p, \bar{p}, e^{+/-}$) generated by the model,

(ii) $(N_a^k)_{sel}^{MC}$ – moment $k = 1, 2$ of particle type a ($a = \pi^{+/-}, K^{+/-}, p, \bar{p}, e^{+/-}$) generated by the model with the detector response simulation, reconstruction and selection,

(iii) $(N_{ab})_{gen/sel}^{MC}$ – mixed second moment of particle types a and b generated by the model (*gen*) and with the detector response simulation, reconstruction and selection (*sel*).

This way of implementing correction was tested on Epos and Venus models. For details see Sec. 9.5. The correction factors for first, second and mixed moments of identified hadrons are shown in Figs. 9, 10 and 11.

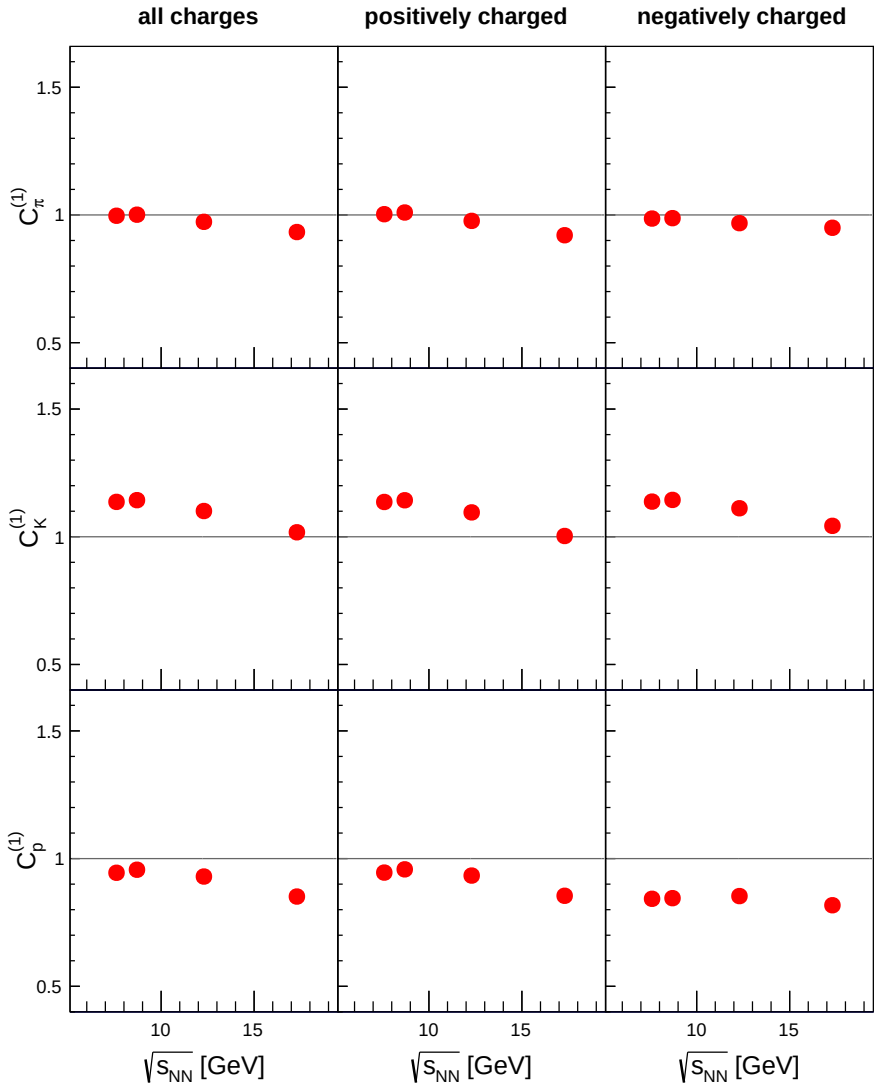

Figure 9: (Color online) Energy dependence of correction factor $C_a^{(1)}$ for all charged, positively and negatively charged pions, kaons and protons.

9.2 Statistical uncertainties

The *sub-sample method* was used to calculate statistical uncertainties of final results. All selected events were grouped into $M = 30$ non-overlapping sub-samples of events. Then a given fluctuation measure Q (for example $\Sigma[\pi^+, p]$) was calculated for each sub-sample separately, and the variance of its distribution, $Var[Q]$, was obtained. The statistical uncertainty of Q for all selected events was estimated as $\sqrt{Var[Q]/M}$. The dE/dx parametrization requires a minimum number of tracks in a p_{lab}, p_{T} bin, thus

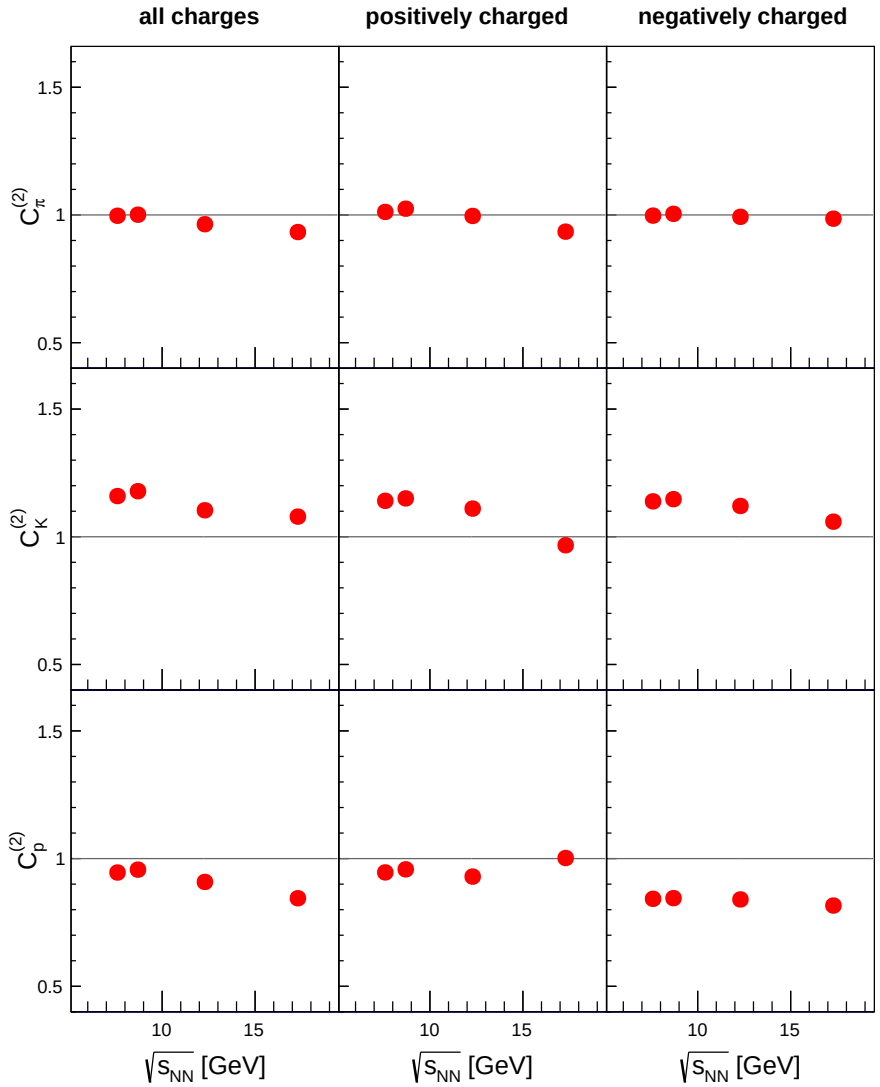

Figure 10: (Color online) Energy dependence of correction factor $C_a^{(2)}$ for all charged, positively and negatively charged pions, kaons and protons.

the acceptance in which the dE/dx parametrization can be obtained is larger for all selected events than for sub-samples of events. In order to have the maximum acceptance the same dE/dx parametrization obtained using all events was used in the sub-sample analysis. It was checked using the *bootstrap method* [35, 36] that the above approximation leads only to a small underestimation of statistical uncertainties.

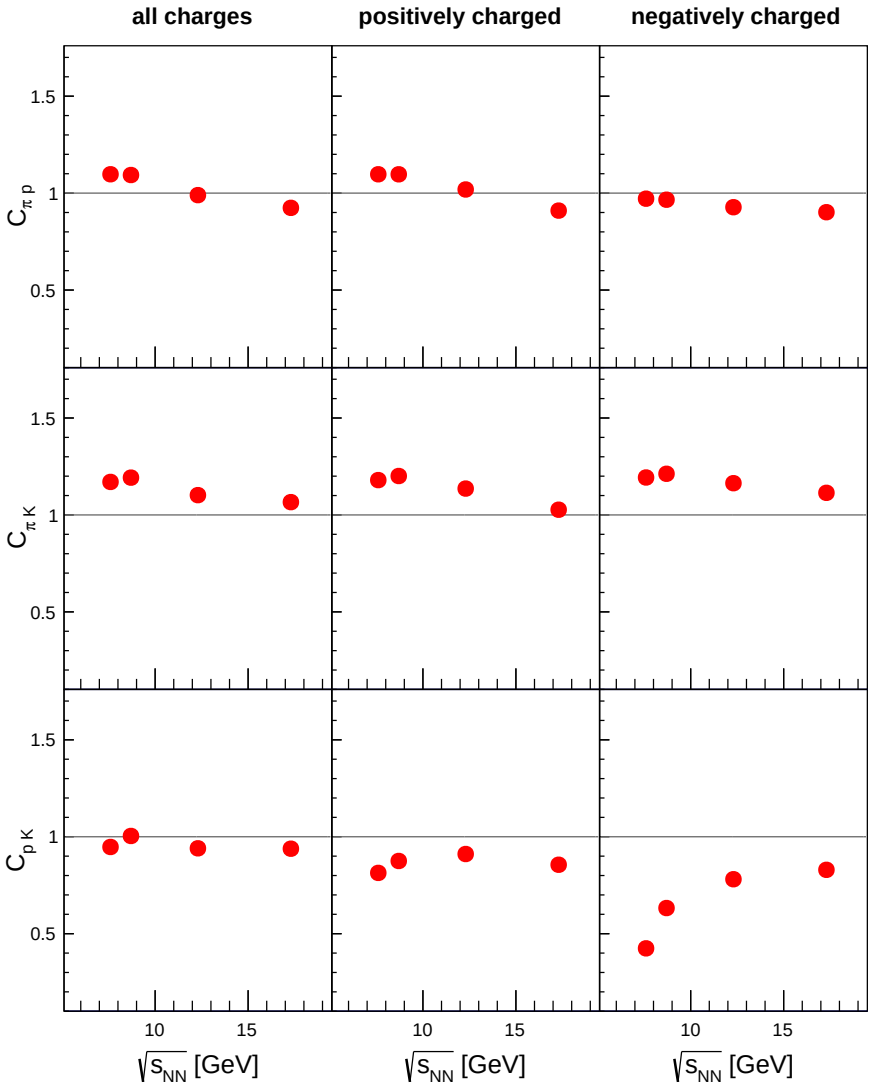

Figure 11: (Color online) Energy dependence of correction factor C_{ab} for all charged, positively and negatively charged combinations of $\pi(p+\bar{p})$, πK and pK.

9.3 Systematic uncertainties

Systematic uncertainties originate from uncertainties of the detector response simulation and models used for calculation of corrections. The total systematic uncertainties were calculated by adding detector-related and model-related contributions in quadrature.

9.4 Detector related effects: event and track selection

These uncertainties were studied by applying standard (see Sec. 7) and loose cuts (see below). For each choice the complete analysis was repeated including the dE/dx fitting. The uncertainties are related to imperfectness of the reconstruction procedure and to the acceptance of events with additional tracks from off-time particles. This systematic uncertainty was estimated by reducing the width of the time window in which no off-time beam particles are allowed from 1.5 μs to 0.5 μs, by relaxing the maximum allowed distance between fitted z position of the vertex and the center of the LHT from ±20 cm to ±40 cm, the requirement on the number of measured points along the track from 30 to 20 (also dE/dx points needed for the fitting) and loosening the constraint on the distance of the track extrapolated back to the target plane and the main vertex from 4 to 8 cm and from 2 to 4 cm in the$x$ and y directions, respectively.

An additional possible source of uncertainty is imperfectness of the dE/dx parametrization. Here the largest uncertainty comes from uncertainties of the parameters of the kaon dE/dx distribution. The kaon distribution significantly overlaps with the proton and pion distributions. In the most difficult low momentum range the dE/dx fits were cross-checked using the time-of-flight information and found to be in agreement at the level of single particle spectra (see Ref. [26]).

In this analysis, as it considers second order moments, two additional tests were performed. First, fits of dE/dx distributions with fixed asymmetry parameter and without any constraint on asymmetry were used to estimate the possible biases of fluctuation measures. The change of the results is below 10% for most quantities. Larger relative differences appear only for quantities close to 0. The second test was performed to validate fit stability. The value of dE/dx for each reconstructed track in the Monte-Carlo simulation was generated using the parametrization of dE/dx response fitted to the data. Next, dE/dx fits were performed on reconstructed Epos1.99 simulated events. Intensive and strongly intensive quantities were obtained the same way as in the data and compared to the values obtained in the model without dE/dx simulation. The change of the results is below 10% for most quantities and, for almost all, it is within or comparable to systematic uncertainty. The only exceptions are the scaled variance of protons at 158 GeV/c (10% which normally is 5%) and pions at 31 GeV/c (15% which normally is 8%) as well as Δ of pions and protons at 158 GeV/c (17% compared to 11%).

Uncertainty related to the selection for the event and track cuts is the main source (about 50%) of the total systematic uncertainty, σ_{sys}, for the majority of the presented results (86 out of 140 measured quantities).

Beam momentum [GeV/c]	$\langle\pi\rangle_{acc}$	$\langle\pi\rangle$	$\langle K\rangle_{acc}$	$\langle K\rangle$	$\langle p+\bar{p}\rangle_{acc}$	$\langle p+\bar{p}\rangle$
31	0.397(1)	3.556(37)	0.0440(3)	0.202(11)	0.280(1)	0.982(3)
40	0.6233(3)	4.101(36)	0.0680(3)	0.254(11)	0.331(1)	1.101(3)
80	1.416(1)	4.701(38)	0.1563(3)	0.296(11)	0.369(1)	1.111(4)
158	2.360(2)	5.514(45)	0.2597(4)	0.366(18)	0.399(1)	1.194(10)

Table 2: Comparison of mean multiplicity in the analysis acceptance to mean multiplicity of identified hadrons in the full phase-space (only statistical uncertainty indicated) [26].

9.5 Choice of models

The procedure applied to correct data and the lack of precise knowledge of the production cross section of weakly decaying particles leads to systematic uncertainty. The uncertainty was estimated using simulations preformed within the Epos1.99 and Venus4.12 models. The simulated Epos data were corrected using corrections obtained based on the Venus model and compared to the unbiased Epos results. Then the same procedure was repeated swapping Epos and Venus. The differences between the unbiased and simulated-corrected results were added to the systematic uncertainty. They are in average about 20% (Epos data) and 25% (Venus data) of σ_{sys}. Note the models show similar agreement with results on p+p interactions at the CERN SPS energies.

10 Results, discussion and comparison with models

In this section final experimental results are presented and discuss as well as compared with predictions of selected string-hadronic models.

10.1 Results

The final results presented in this section refer to identified hadrons produced in inelastic p+p interactions by strong interaction processes and in electromagnetic decays of produced hadrons. They were obtained within the kinematic acceptances given in Ref. [32] and illustrated in Fig. 4. Note, that the kinematic acceptances for positively and negatively charged hadrons are different.

Mean multiplicities of pions, kaons and anti-protons in the acceptance region of the fluctuation analysis are plotted in Fig. 12 and compared to corresponding mean multiplicities measured in the full phase-space in Table 2.

Pions are the most abundantly produced particles and they are the majority of accepted charged hadrons in all analyzed reactions. With decreasing beam momentum the contribution of protons increases and small contributions of kaons and anti-protons decrease. Almost all negatively charged hadrons are pions,

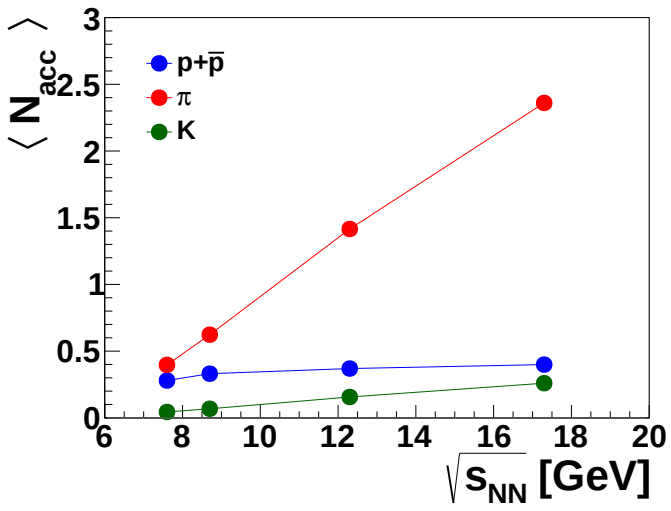

Figure 12: (Color online) Mean multiplicities of charged π, K and $p + \bar{p}$ in the analysis acceptance as a function of collision energy. Only statistical uncertainties are shown.

whereas protons are majority of positively charged hadrons at the lowest beam momentum, 31 GeV/c. The changes of particle type composition with charge of selected hadrons and beam momentum are related to different thresholds for production of pions, kaons and anti-protons. Mean proton multiplicity in the full phase-space is about one (0.3-0.4 in the acceptance) and it is approximately independent of beam momentum. This is because final state protons are strongly correlated with two initial state protons via the baryon number conservation.

Figure 13 shows the collision energy dependence of the scaled variance of pion, kaon and proton multiplicity distributions. Note, the intensive fluctuation measure ω is one for a Poisson distribution and zero in the case of a constant multiplicity for all collisions. The scaled variance quantifies the width of the multiplicity distribution relatively to the width of the Poisson distribution with the same mean multiplicity. The results for all charged, positively charged and negatively charged hadrons are presented separately. One observes:

(i) ω for pions increases with the collision energy. The increase is the strongest for all charged pions. This is likely to be related to the well established KNO scaling of the charged hadron multiplicity distributions in inelastic p+p interactions with the scaled variance being proportional to mean multiplicity [37, 38, 39]. Global and local (resonance decays) electric charge conservation correlates multiplicities of positively and negatively charged pions and thus the effect is the most pronounced for all charged hadrons.

(ii) The dependence of ω on beam momentum and hadron charge for kaons is qualitatively similar to the one for pions but weaker. This is probably related with a significantly smaller mean multiplicity of kaons than pions. One notes that scaled variance of a single maximum multiplicity distribution

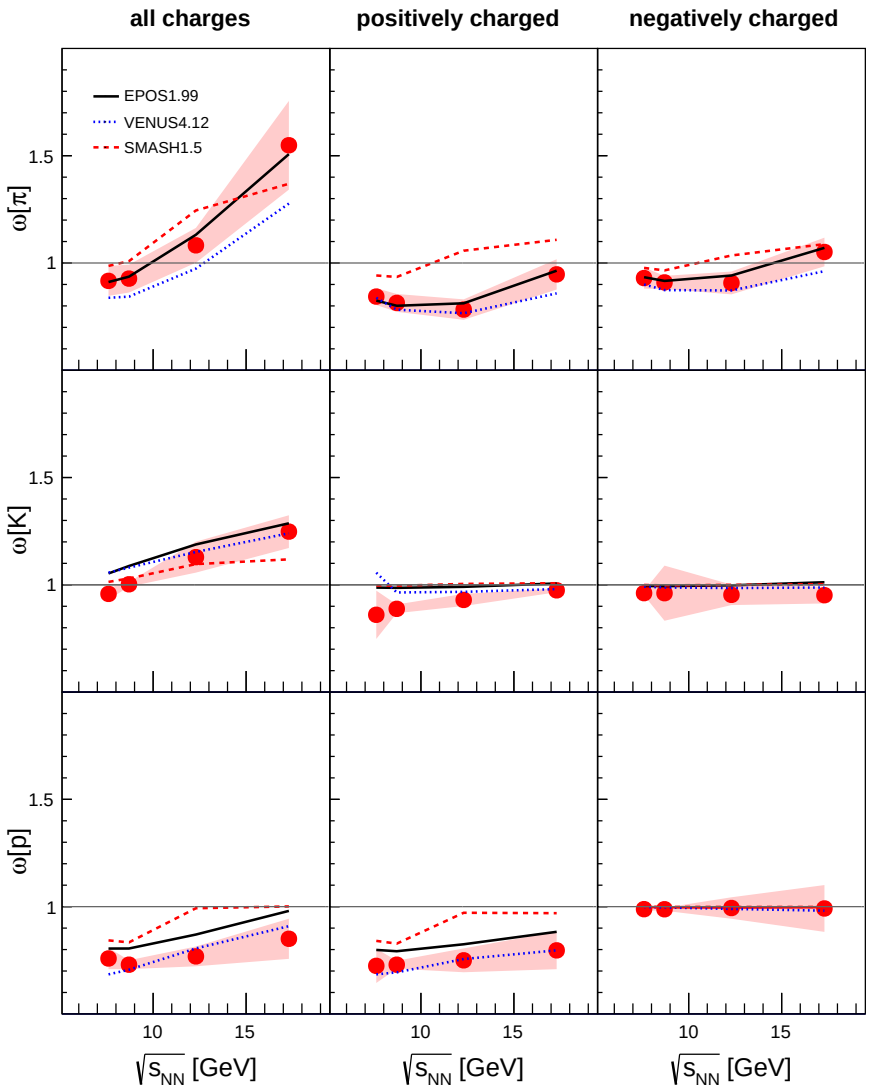

Figure 13: (Color online) The collision energy dependence of scaled variance of pion, kaon and protons produced in inelastic p+p interactions. Results for all charged, positively and negatively charged hadrons are presented separately. The solid, dashed and dotted lines show predictions of Epos1.99, Smash1.5 and Venus4.12 models, respectively. Statistical uncertainty is denoted with bar and systematic uncertainty is indicated with red band.

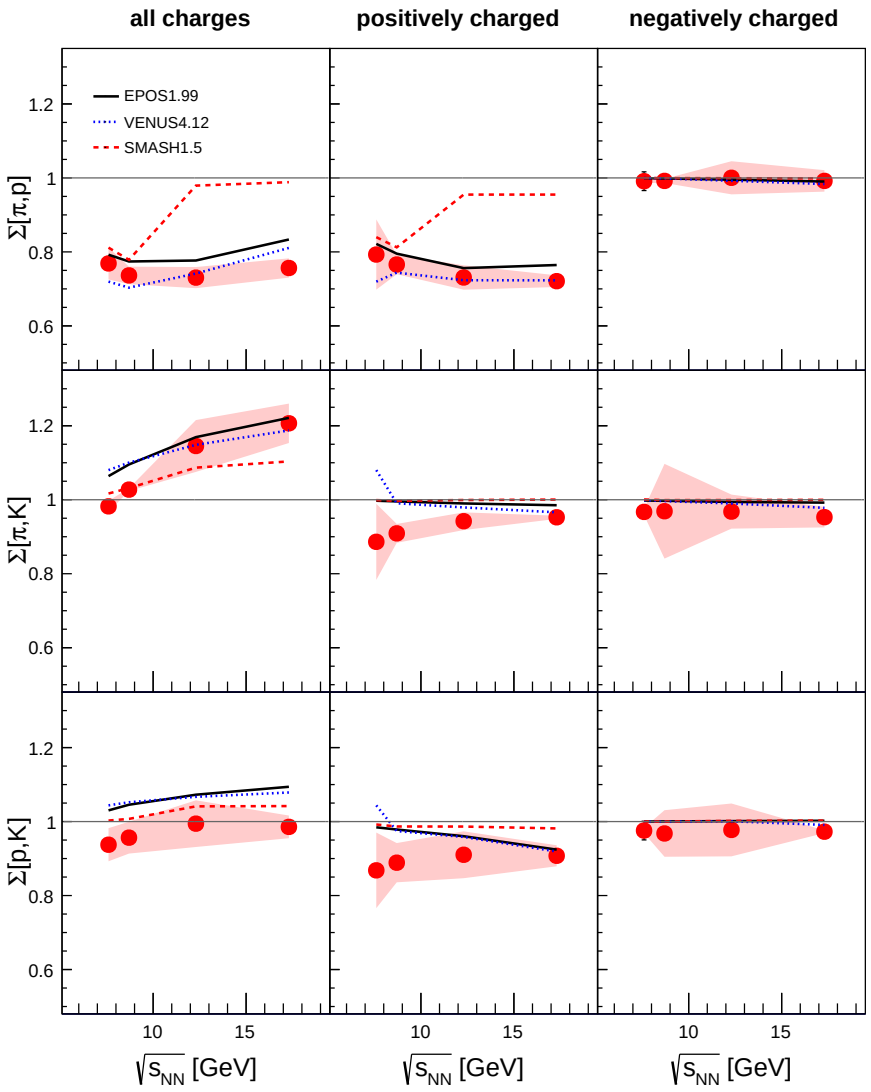

Figure 14: (Color online) The collision energy dependence of $\Sigma[\pi, (p+\overline{p})]$, $\Sigma[\pi, K]$ and $\Sigma[(p+\overline{p}), K]$ in inelastic p+p interactions. Results for all charged, positively and negatively charged hadrons are presented separately. The solid, dashed and dotted lines show predictions of Epos1.99, Smash1.5 and Venus4.12 models, respectively. Statistical uncertainty is denoted with bar and systematic uncertainty is indicated with red band.

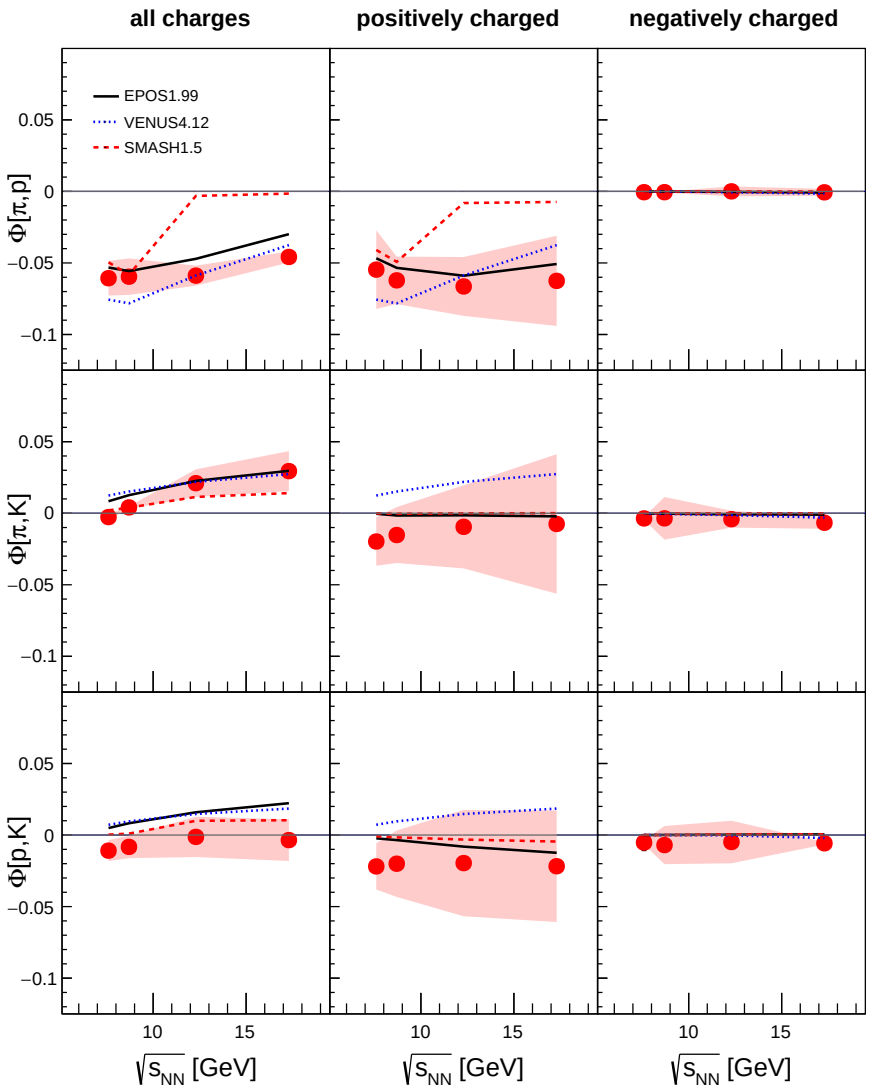

Figure 15: (Color online) The collision energy dependence of $\Phi[\pi,(p+\overline{p})]$, $\Phi[\pi,K]$ and $\Phi[(p+\overline{p}),K]$ in inelastic p+p interactions. Results for all charged, positively and negatively charged hadrons are presented separately. The solid, dashed and dotted lines show predictions of Epos1.99, Smash1.5 and Venus4.12 models, respectively. Statistical uncertainty is denoted with bar and systematic uncertainty is indicated with red band.

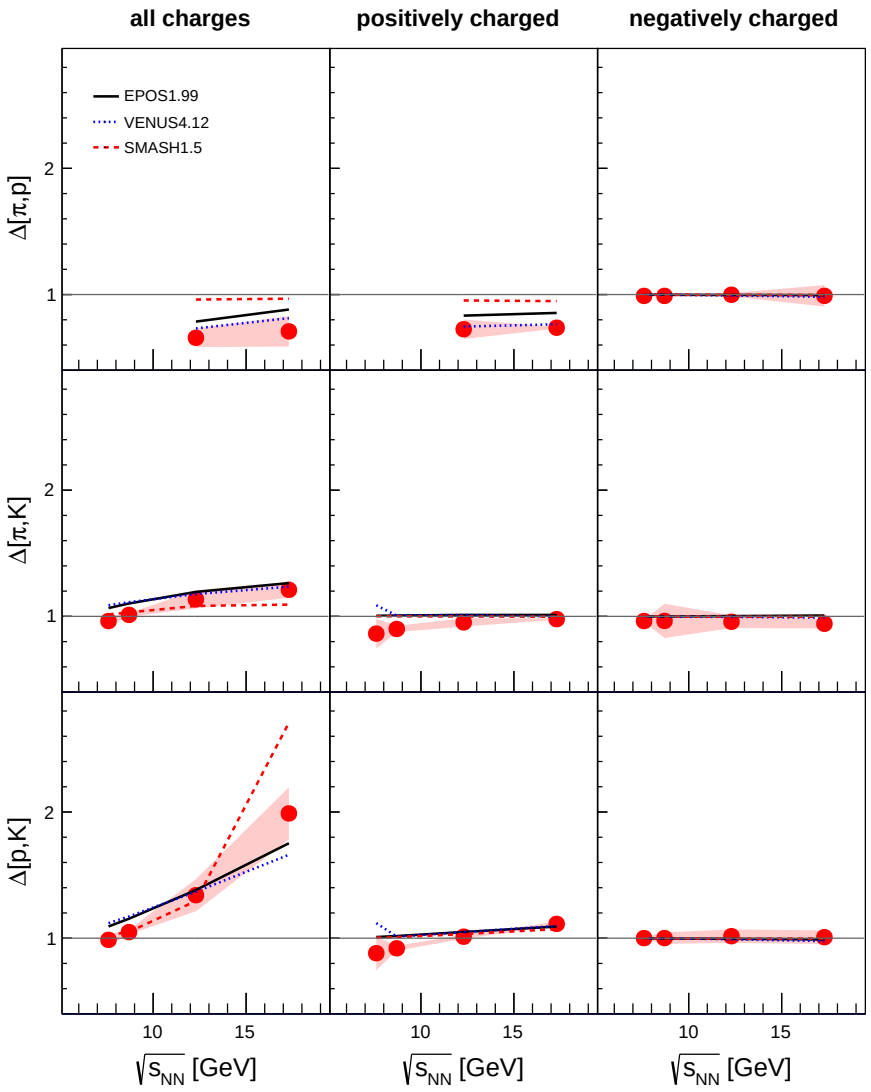

Figure 16: (Color online) The collision energy dependence of $\Delta[\pi,(p+\overline{p})]$, $\Delta[\pi,K]$ and $\Delta[(p+\overline{p}),K]$ in inelastic p+p interactions. Results for all charged, positively and negatively charged hadrons are presented separately. The solid, dashed and dotted lines show predictions of Epos1.99, Smash1.5 and Venus4.12 models, respectively. Statistical uncertainty is denoted with bar and systematic uncertainty is indicated with red band.

approaches one with mean multiplicity decreasing to zero. The latter effect is likely responsible for $\omega[K^-]$ and $\omega[\overline{p}]$ being close to one, mean multiplicity of K^- and $\overline{p}$ in the acceptance is below 0.1 and 0.03, respectively.

(iii) The scaled variance of protons is about 0.8 and it weakly depends on the beam momentum. The net-baryon (baryon - anti-baryon) multiplicity in the full phase-space is exactly two. This is because the initial baryon number is two and the baryon number conservation. Thus the scaled variance of the net-baryon multiplicity distribution is zero. The anti-baryon production at the SPS energies is small and thus the net-baryon multiplicity is close to the baryon multiplicity. The baryons are predominately protons and neutrons. Thus the proton fluctuations are expected to be mostly due to fluctuation of the proton to neutron ratio and fluctuations caused by the limited acceptance of protons.

Figures 14 and 15 show the results on Σ and Φ for pion-proton, pion-kaon and proton-kaon multiplicities measured separately for all charged, positively charged, and negatively charged hadrons produced in inelastic p+p collisions at 31–158 GeV/c beam momentum. The strongly intensive measures Σ and Φ differ only by a selection of the reference value (one for Σ and zero for Φ) and a normalization factor which involves mean multiplicities, see Eq. 3. They are both presented here due to historical reasons, but only results for Σ are discussed. The Σ measure assumes value one in the Independent Particle Production Model which postulates that particle types are attributed to particles independent of each other. This implies that Σ unlike ω is insensitive to particle multiplicity distribution. One observes:

(i) For all and positively charged pions-protons Σ is significantly below one (approximately 0.8) and it is weakly dependent on the beam momentum. This is likely due to a large fraction of pion-proton pairs coming from decays of baryonic resonances [40, 41].

(ii) Σ for all charge pions-kaons increases significantly with the beam momentum and it is about 1.2 at 158 GeV/c. The origin of this behaviour is unclear.

(iii) For remaining cases Σ is somewhat below or close to one suggesting a small contribution of hadrons from resonance decays.

Figure 16 shows the results for Δ of identified hadrons calculated separately for all charged, positively charged, and negatively charged hadrons produced in inelastic p+p collisions at beam momenta from 31 to 158 GeV/c. The general properties of Δ are similar to the properties of Σ discussed above. Unlike Σ, Δ does not include a correlation term between multiplicities of two hadron types, see Eqs. 1 and 2. One observes:

(i) Δ for all and positively charged pions and protons is below one. It is qualitatively similar to Σ and thus likely to be caused by resonance decays.

(ii) $\Delta[(p + \bar{p}), K]$ increases with the collision energy from about one to two. The origin of this dependence is unclear.

10.2 Comparison with models

The results shown in Figs. 13, 14, 15 and 16 are compared with predictions of three string-resonance models: Epos1.99 [30, 31] (solid lines), Smash1.5 (dashed lines) [42] and Venus4.12 [43, 44] (dotted lines).

None of the models agree with all presented results. In a number of cases qualitative disagreement is observed. These models are supposed to define the baseline for heavy ion collisions from which any critical phenomena are expected to emerge. However, the models should first be tuned to the experimental data on p+p interactions presented here. In p+p interactions at CERN SPS energies one expects none of the high matter density phenomena usually studied and searched for in nucleus-nucleus collisions. Any deviations from independent particle production are considered to be caused by well established effects discussed in Sec. 10.1.

11 Summary and outlook

In this paper experimental results on multiplicity fluctuations of identified hadrons produced in inelastic p+p interactions at 31, 40, 80, and 158 GeV/c beam momentum are presented. Four different measures of multiplicity fluctuations are used: the scaled variance ω and the strongly intensive measures Σ, Φ and Δ. The fluctuation measures involve second and first moments of joint multiplicity distributions. Data analysis was preformed using the Identity method which corrects for incomplete particle identification. Strongly intensive quantities are calculated in order to allow for a direct comparison with corresponding results on nucleus-nucleus collisions. The results for different hadron types are shown as a function of collision energy.

The measurements of NA61/SHINE were compared with string-resonance models Smash1.5, Epos1.99 and Venus4.12. None of the models agree with all presented results. In a number of cases qualitative disagreement is observed. Thus, before the models can be used for predicting the baseline for heavy ion collisions in the search for critical phenomena, the models need to be tuned to the experimental data on p+p interactions presented in this paper.

Acknowledgements

We would like to thank the CERN EP, BE, HSE and EN Departments for the strong support of NA61/SHINE.

This work was supported by the Hungarian Scientific Research Fund (grant NKFIH 123842/123959), the Polish Ministry of Science and Higher Education (grants 667/N-CERN/2010/0, NN 202 48 4339 and NN 202 23 1837), the National Science Centre Poland (grants 2014/14/E/ST2/00018, 2014/15/B/ST2 / 02537 and 2015/18/M/ST2/00125, 2015/19/N/ST2 /01689, 2016/23/B/ST2/00692, 2017/ 25/N/ ST2/ 02575, 2018/30/A/ST2/00226, 2018/31/G/ST2/03910), WUT ID-UB, the Russian Science Foundation, grant 16-12-10176 and 17-72-20045, the Russian Academy of Science and the Russian Foundation for Basic Research (grants 08-02-00018, 09-02-00664 and 12-02-91503-CERN), the Russian Foundation for Basic Research (RFBR) funding within the research project no. 18-02-00086, the National Research Nuclear University MEPhI in the framework of the Russian Academic Excellence Project (contract No. 02.a03.21.0005, 27.08.2013), the Ministry of Science and Higher Education of the Russian Federation, Project "Fundamental properties of elementary particles and cosmology" No 0723-2020-0041, the European Union's Horizon 2020 research and innovation programme under grant agreement No. 871072, the Ministry of Education, Culture, Sports, Science and Technology, Japan, Grant-in-Aid for Scientific Research (grants 18071005, 19034011, 19740162, 20740160 and 20039012), the German Research Foundation (grant GA 1480/8-1), the Bulgarian Nuclear Regulatory Agency and the Joint Institute for Nuclear Research, Dubna (bilateral contract No. 4799-1-18/20), Bulgarian National Science Fund (grant DN08/11), Ministry of Education and Science of the Republic of Serbia (grant OI171002), Swiss Nationalfonds Foundation (grant 200020117913/1), ETH Research Grant TH-01 07-3 and the Fermi National Accelerator Laboratory (Fermilab), a U.S. Department of Energy, Office of Science, HEP User Facility managed by Fermi Research Alliance, LLC (FRA), acting under Contract No. DE-AC02-07CH11359 and the IN2P3-CNRS (France).

References

[1] N. Abgrall *et al.*, [NA61/SHINE Collab.] *JINST* **9** (2014) P06005.

[2] A. Aduszkiewicz, [NA61/SHINE Collab.], "Report from the NA61/SHINE experiment at the CERN SPS," Tech. Rep. CERN-SPSC-2018-029. SPSC-SR-239, CERN, 2018.

[3] M. Gazdzicki and S. Mrowczynski *Z. Phys.* **C54** (1992) 127.

[4] M. Gorenstein and M. Gazdzicki *Phys. Rev.* **C84** (2011) 014904.

[5] M. Gazdzicki, M. Gorenstein, and M. Mackowiak-Pawlowska *Phys. Rev.* **C88** (2013) 024907.

[6] T. Anticic *et al.*, [NA49 Collab.] *Phys. Rev.* **C70** (2004) 034902.

[7] T. Anticic *et al.*, [NA49 Collab.] *Phys. Rev.* **C79** (2009) 044904.

[8] C. Alt *et al.*, [NA49 Collab.] *Phys. Rev.* **C70** (2004) 064903.

[9] T. Anticic *et al.*, [NA49 Collab.] *Phys. Rev.* **C89** (2014) 054902.

[10] C. Alt *et al.*, [NA49 Collab.] *Phys. Rev.* **C75** (2007) 064904.

[11] C. Alt *et al.*, [NA49 Collab.] *Phys. Rev.* **C78** (2008) 034914.

[12] T. Anticic *et al.*, [NA49 Collab.] *Phys. Rev.* **C92** (2015) 044905.

[13] A. Aduszkiewicz *et al.*, [NA61/SHINE Collab.] *Eur. Phys. J.* **C76** (2016) 635.

[14] M. Gazdzicki, K. Grebieszkow, M. Mackowiak, and S. Mrowczynski *Phys. Rev.* **C83** (2011) 054907.

[15] M. Gorenstein *Phys. Rev.* **C84** (2011) 024902.

[16] A. Rustamov and M. Gorenstein *Phys. Rev.* **C86** (2012) 044906.

[17] C. A. Pruneau *Phys. Rev.* **C96** (2017) 054902.

[18] M. Mackowiak-Pawlowska and P. Przybyla *Eur. Phys. J.* **C78** (2018) 391.

[19] C. A. Pruneau and A. Ohlson *Phys. Rev.* **C98** (2018) 014905.

[20] M. Mackowiak-Pawlowska, [NA61 Collab.] *PoS* **CPOD2013** (2013) 048.

[21] S. Acharya *et al.*, [ALICE Collab.] *Eur. Phys. J.* **C79** no. 3, (2019) 236.

[22] A. Rustamov, [ALICE Collab.] *Nucl. Phys.* **A967** (2017) 453–456.

[23] S. Acharya *et al.*, [ALICE Collab.] *Phys. Lett. B* **807** (2020) 135564, `arXiv:1910.14396 [nucl-ex]`.

[24] A. Bialas, M. Bleszynski, and W. Czyz *Nucl. Phys.* **B111** (1976) 461.

[25] N. Abgrall *et al.*, [NA61/SHINE Collab.] *Eur. Phys. J.* **C74** (2014) 2794.

[26] A. Aduszkiewicz *et al.*, [NA61/SHINE Collab.] *Eur. Phys. J.* **C77** no. 10, (2017) 671.

[27] N. Abgrall *et al.*, [NA61 Collab.], "Calibration and analysis of the 2007 data," 2008. CERN-SPSC-2008-018, CERN-SPSC-SR-033.

[28] N. Abgrall *et al.*, [NA61/SHINE Collab.] *Phys. Rev.* **C84** (2011) 034604.

[29] M. Unger, [NA61/SHINE Collab.] *EPJ Web Conf.* **52** (2013) 01009.

[30] K. Werner *Nucl. Phys. Proc. Suppl.* **175-176** (2008) 81–87.

[31] T. Pierog, C. Baus, R. Ulrich, Cosmic Ray Monte Carlo package, https://web.ikp.kit.edu/rulrich/crmc.html.

[32] NA61/SHINE acceptance for these analysis available at https://edms.cern.ch/document/2228711/1.

[33] M. van Leeuwen, [NA49 Collab.] arXiv:nucl-ex/0306004 [nucl-ex].

[34] M. van Leeuwen, "A practical guide to dE/dx analysis in NA49" (2008) https://edms.cern.ch/document/983015/2.

[35] B. Efron *The Annals of Statistics* **7** (1979) 1–26.

[36] T. C. Hesterberg, D. S. Moore, S. Monaghan, A. Clipson, and R. Epstein, "Bootstrap methods and permutation tests," 2005. http://bcs.whfreeman.com/ips5e/content/cat_080/pdf/moore14.pdf.

[37] Z. Koba, H. B. Nielsen, and P. Olesen *Nucl. Phys.* **B40** (1972) 317–334.

[38] A. Golokhvastov *Phys. Atom. Nucl.* **64** (2001) 1841–1855.

[39] A. Golokhvastov *Phys. Atom. Nucl.* **64** (2001) 84–97.

[40] V. V. Begun, M. I. Gorenstein, and K. Grebieszkow *J. Phys. G* **42** (2015) 075101.

[41] M. Gorenstein *PoS* **CPOD2014** (2015) 017.

[42] J. Weil *et al. Phys. Rev.* **C94** (2016) 054905.

[43] K. Werner *Phys. Rept.* **232** (1993) 87–299.

[44] K. Werner *Nucl. Phys.* **A525** (1991) 501–506.

The NA61/SHINE Collaboration

A. Acharya[9], H. Adhikary[9], A. Aduszkiewicz[15], E.V. Andronov[21], T. Antićić[3], V. Babkin[19], M. Baszczyk[13], S. Bhosale[10], A. Blondel[4], M. Bogomilov[2], A. Brandin[20], A. Bravar[23], W. Bryliński[17], J. Brzychczyk[12], M. Buryakov[19], O. Busygina[18], A. Bzdak[13], H. Cherif[6], M. Ćirković[22], M. Csanad [7], J. Cybowska[17], T. Czopowicz[9,17], A. Damyanova[23], N. Davis[10], M. Deliyergiyev[9], M. Deveaux[6], A. Dmitriev [19], W. Dominik[15], P. Dorosz[13], J. Dumarchez[4], R. Engel[5], G.A. Feofilov[21], L. Fields[24], Z. Fodor[7,16], A. Garibov[1], M. Gaździcki[6,9], O. Golosov[20], V. Golovatyuk [19], M. Golubeva[18], K. Grebieszkow[17], F. Guber[18], A. Haesler[23], S.N. Igolkin[21], S. Ilieva[2], A. Ivashkin[18], S.R. Johnson[25], K. Kadija[3], N. Kargin[20], E. Kashirin[20], M. Kiełbowicz[10], V.A. Kireyeu[19], V. Klochkov[6], V.I. Kolesnikov[19], D. Kolev[2], A. Korzenev[23], V.N. Kovalenko[21], S. Kowalski[14], M. Koziel[6], A. Krasnoperov[19], W. Kucewicz[13], M. Kuich[15], A. Kurepin[18], D. Larsen[12], A. László[7], T.V. Lazareva[21], M. Lewicki[16], K. Łojek[12], V.V. Lyubushkin[19], M. Maćkowiak-Pawłowska[17], Z. Majka[12], B. Maksiak[11], A.I. Malakhov[19], A. Marcinek[10], A.D. Marino[25], K. Marton[7], H.-J. Mathes[5], T. Matulewicz[15], V. Matveev[19], G.L. Melkumov[19], A.O. Merzlaya[12], B. Messerly[26], Ł. Mik[13], S. Morozov[18,20], S. Mrówczyński[9], Y. Nagai[25], M. Naskręt[16], V. Ozvenchuk[10], V. Paolone[26], O. Petukhov[18], R. Płaneta[12], P. Podlaski[15], B.A. Popov[19,4], B. Porfy[7], M. Posiadała-Zezula[15], D.S. Prokhorova[21], D. Pszczel[11], S. Puławski[14], J. Puzović[22], M. Ravonel[23], R. Renfordt[6], D. Röhrich[8], E. Rondio[11], M. Roth[5], B.T. Rumberger[25], M. Rumyantsev[19], A. Rustamov[1,6], M. Rybczynski[9], A. Rybicki[10], S. Sadhu[9], A. Sadovsky[18], K. Schmidt[14], I. Selyuzhenkov[20], A.Yu. Seryakov[21], P. Seyboth[9], M. Słodkowski[17], P. Staszel[12], G. Stefanek[9], J. Stepaniak[11], M. Strikhanov[20], H. Ströbele[6], T. Šuša[3], A. Taranenko[20], A. Tefelska[17], D. Tefelski[17], V. Tereshchenko[19], A. Toia[6], R. Tsenov[2], L. Turko[16], R. Ulrich[5], M. Unger[5], D. Uzhva[21], F.F. Valiev[21], D. Veberič[5], V.V. Vechernin[21], A. Wickremasinghe[26,24], Z. Włodarczyk[9], K. Wojcik[14], O. Wyszyński[9], E.D. Zimmerman[25], and R. Zwaska[24]

[1] National Nuclear Research Center, Baku, Azerbaijan

[2] Faculty of Physics, University of Sofia, Sofia, Bulgaria

[3] Ruđer Bošković Institute, Zagreb, Croatia

[4] LPNHE, University of Paris VI and VII, Paris, France

[5] Karlsruhe Institute of Technology, Karlsruhe, Germany

[6] University of Frankfurt, Frankfurt, Germany

[7] Wigner Research Centre for Physics of the Hungarian Academy of Sciences, Budapest, Hungary

[8] University of Bergen, Bergen, Norway

[9] Jan Kochanowski University in Kielce, Poland

[10] Institute of Nuclear Physics, Polish Academy of Sciences, Cracow, Poland

[11] National Centre for Nuclear Research, Warsaw, Poland

[12] Jagiellonian University, Cracow, Poland

[13] AGH - University of Science and Technology, Cracow, Poland

[14] University of Silesia, Katowice, Poland
[15] University of Warsaw, Warsaw, Poland
[16] University of Wrocław, Wrocław, Poland
[17] Warsaw University of Technology, Warsaw, Poland
[18] Institute for Nuclear Research, Moscow, Russia
[19] Joint Institute for Nuclear Research, Dubna, Russia
[20] National Research Nuclear University (Moscow Engineering Physics Institute), Moscow, Russia
[21] St. Petersburg State University, St. Petersburg, Russia
[22] University of Belgrade, Belgrade, Serbia
[23] University of Geneva, Geneva, Switzerland
[24] Fermilab, Batavia, USA
[25] University of Colorado, Boulder, USA
[26] University of Pittsburgh, Pittsburgh, USA